Transient natural convection in a rectangular enclosure with one heated side wall

John D. Hall
The Deringer Group, 335 Cove Road, Riva, MD 21140, USA

Adrian Bejan and Jack B. Chaddock
Department of Mechanical Engineering and Materials Science,
Duke University, Durham, NC 27706, USA

Received October 1987 and accepted for publication February 1988

This paper describes a numerical and theoretical study of the transient natural convection heating of a two-dimensional rectangular enclosure filled with fluid. The heating is applied suddenly along one of the side walls, while the remaining three walls are maintained insulated. It is shown that the process has two distinct phases, an early period dominated by conduction and a late period dominated by convection. The scaling laws for the heat transfer rate and the effectiveness (energy storage fraction) are determined based on scale analysis. These theoretical results are confirmed by numerical experiments conducted in the domain $Ra = 10^3$–10^6, $Pr = 7$, $A = 1$, where Ra is the Rayleigh number based on height and initial temperature difference, Pr is the Prandtl number, and A is the height/length ratio of the enclosure. Correlations for heat transfer rate and effectiveness are constructed by comparing the theoretical scaling laws with the numerical results.

Keywords: transient natural convection; numerical experiments; scale analysis

Introduction

Despite the deluge of publications on natural convection heat transfer of the past decade, the literature shows that there have been relatively few studies of the fundamentals of transient natural convection in enclosures. This state of affairs seems surprising if we consider the fact that most of the confined flows driven by buoyancy in architectural, environmental, and solar energy engineering applications are time-dependent. One possible explanation for the almost exclusive coverage of steady-state natural convection in enclosures is that the steady state is simpler, easier, and safer as a research topic than its transient counterpart. The latter turns out to be one of the more controversial topics in natural convection today.[1–6]

In the present study we document the most basic features of the phenomenon of transient natural convection in an enclosure by focusing on what is perhaps the simplest configuration in which the phenomenon can be studied. This configuration is the two-dimensional rectangular enclosure shown in Figure 1, in which one side wall is suddenly heated to the new temperature T_h while the remaining three walls are perfectly insulated. In the initial state the fluid that fills the enclosure is motionless and isothermal at temperature T_i. The study is a combination of numerical experiments and scale analysis whose chief engineering objective is to produce scaling-correct correlations for the evolution of the heat transfer rate and bulk temperature of the enclosed fluid.

Among the few studies that have addressed the general topic, a prominent position is occupied by Patterson and Imberger's paper.[1] They treat a configuration related to that of Figure 1, in which the right wall is cooled suddenly at the same time as the left wall is heated. Several of Patterson and Imberger's scaling results apply to the present problem as well; therefore, they are identified and adopted at various stages in the presentation that follows. The controversy that accompanies the topic of transient natural convection in enclosures is illustrated by the more recent experimental studies[2–5] and by Patterson's[6] refinement of the original scaling theory.[1] One purely numerical study that addressed the same configuration as the one shown in Figure 1 was published recently by Nicolette *et al.*[7] The theoretical component (scale analysis) of the present paper is offered therefore as an explanation for Nicolette *et al.*'s observations as well as for our own numerical experiments.

Mathematical formulation

The fluid that fills the two-dimensional cavity of Figure 1 was modeled as Newtonian, Boussinesq-incompressible, and with constant thermophysical properties. The Boussinesq-incompressible assumption means that the density is regarded as a constant in the course of writing the governing equations, the only exception to this rule being the buoyancy term of the momentum equation, in which the density is assumed to decrease linearly as the temperature increases.

The vorticity–stream function formulation of the dimension-

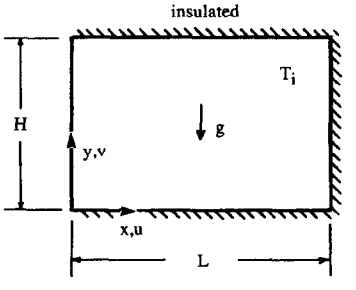

Figure 1 Two-dimensional enclosure heated along the left wall

less momentum and energy equations is

$$\mathrm{Pr}^{-1}\frac{\partial\Omega}{\partial\tau}+U\frac{\partial\Omega}{\partial X}+V\frac{\partial\Omega}{\partial Y}=\nabla^2\Omega+\frac{\mathrm{Ra}}{\mathrm{Pr}}\frac{\partial\theta}{\partial X} \tag{1}$$

$$\Omega=-\nabla^2\Psi \tag{2}$$

$$\mathrm{Pr}^{-1}\frac{\partial\theta}{\partial\tau}+U\frac{\partial\theta}{\partial X}+V\frac{\partial\theta}{\partial Y}=\mathrm{Pr}^{-1}\nabla^2\theta \tag{3}$$

where $\nabla^2=\partial^2/\partial X^2+\partial^2/\partial Y^2$. The dimensionless variables that appear in these equations are defined by the relations

$$X=\frac{x}{H},\qquad Y=\frac{y}{H} \tag{4}$$

$$U=\frac{u}{\nu/H},\qquad V=\frac{v}{\nu/H} \tag{5}$$

$$\tau=\frac{t}{H^2/\alpha},\qquad \theta=\frac{T-T_i}{T_h-T_i} \tag{6}$$

$$\Psi=\frac{\psi}{\nu/H^2},\qquad \Omega=\frac{\omega}{\nu} \tag{7}$$

in which the dimensionless variables and thermophysical properties are defined in the Notation. The physical stream function and vorticity are defined in the usual manner by writing $u=\partial\psi/\partial y$, $v=-\partial\psi/\partial x$, and $\omega=\partial v/\partial x-\partial u/\partial y$.

In the numerical experiments that are described next, Equations 1–3 are solved subject to the initial conditions

$$\Psi=0 \quad\text{and}\quad \theta=0 \quad\text{at}\ \tau=0 \tag{8}$$

and the four boundary conditions that are maintained for times $\tau>0$:

$$\Psi=\frac{\partial\Psi}{\partial X}=0 \quad\text{and}\quad \theta=1 \quad\text{at}\ X=0 \tag{9}$$

$$\Psi=\frac{\partial\Psi}{\partial X}=0 \quad\text{and}\quad \frac{\partial\theta}{\partial X}=0 \quad\text{at}\ X=A^{-1}=\frac{L}{H} \tag{10}$$

$$\Psi=\frac{\partial\Psi}{\partial Y}=0 \quad\text{and}\quad \frac{\partial\theta}{\partial Y}=0 \quad\text{at}\ Y=0\ \text{and}\ Y=1 \tag{11}$$

The governing equations and boundary conditions listed above involve three dimensionless groups, namely, the geometric aspect ratio $A=H/L$, the Prandtl number $\mathrm{Pr}=\nu/\alpha$, and the Rayleigh number based on cavity height,

$$\mathrm{Ra}=\frac{g\beta H^3\Delta T}{\alpha\nu} \tag{12}$$

in which $\Delta T=T_h-T_i$.

Numerical procedure

The alternating direction implicit (ADI) method of Peaceman and Rachford[8] was used in order to solve the vorticity and energy equations, Equations 1 and 3. The ADI formulation of these equations is a tridiagonal matrix that can be solved readily using a special adaptation of Gaussian elimination, namely, the Thomas algorithm. ADI was preferred over other methods, because it allows relatively larger time steps. Furthermore, it has second-order accuracy and its weak stability conditions are easier to satisfy. The instabilities are caused by the nonlinear inertia and convection terms of Equations 1 and 3. In order to improve the stability, the nonlinear terms were evaluated using the second upwind differencing method. The stream-function equation 2 was solved by using the successive overrelaxation (SOR) iterative method.

The numerical procedure for any given time step started with determining the temperature field θ by solving Equation 3. The velocity values calculated at the previous time step were used in this phase in order to improve the stability. The next phase involved the use of Equation 1 in order to determine the vorticity field Ω and, finally, the SOR solution to Equation 2 for the stream-function field Ψ. The velocity components at every grid point were then evaluated by invoking the definitions $U=\partial\Psi/\partial Y$ and $V=-\partial\Psi/\partial X$. Next, the fields for θ, Ω, and Ψ were calculated sequentially one more time, using now the

Notation

A	Geometric aspect ratio, H/L
c	Specific heat
c_1, c_2	Empirical constants of order 1
g	Gravitational acceleration
H	Height
k	Thermal conductivity
L	Length (horizontal dimension)
Nu	Nusselt number, Equations 18 and 19
Pr	Prandtl number
Q	Instantaneous overall heat transfer rate, W/m
Ra	Rayleigh number based on ΔT
Ra_*	Rayleigh number based on $\Delta T'$
t	time
t_f	Time scale when the vertical boundary layer becomes convective, Equation 22
t_∞	Time scale when the cavity has absorbed practically all the energy that it can absorb, Equation 34
T	Temperature
T_h	Heated wall temperature, Figure 1
T_i	Initial temperature
ΔT	Initial temperature difference, T_h-T_i
$\Delta T'$	Instantaneous heated wall–bulk fluid temperature difference
u, v	Horizontal and vertical components
U, V	Dimensionless horizontal and vertical velocity components
x, y	Cartesian coordinates, Figure 1
X, Y	Dimensionless Cartesian coordinates

Greek Symbols

α	Thermal diffusivity
β	Coefficient of volumetric thermal expansion
ε	Effectiveness, Equation 21
θ	Dimensionless temperature
ν	Kinematic viscosity
ρ	Density
τ	Dimensionless time, Equation 6
τ_E	Early-period dimensionless time, Equation 26
τ_L	Late-period dimensionless time, Equation 35
ψ	Stream function
Ψ	Dimensionless stream function
ω	Vorticity function
Ω	Dimensionless vorticity function

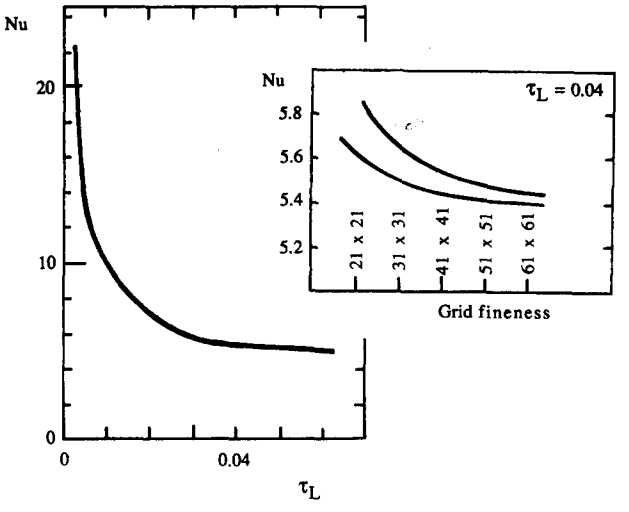

Figure 2 The effect of grid fineness on the heat transfer rate history [Ra = (1.4)10⁴, Pr = 7, $A = 1$]

updated velocity values. This iterative procedure was continued until the θ, Ω, and Ψ values at each grid point converged on what became the "solution" for the given time step. The entire procedure was then repeated for each of the time steps that, taken together, represent the history of the natural convection phenomenon.

The numerical solutions included in this paper correspond to a "high Pr" fluid (water, Pr = 7), as demanded by the theoretical part of the study. In all the computational runs the cavity geometry was square ($A = 1$), while the Rayleigh number varied in the range 10^3–10^6.

All calculations were made using a uniform grid (equidistant mesh) whose fineness was tested carefully for stability and accuracy before final adoption. For example, the cell Reynolds number criterion for stability requires[9]

$$\frac{v\,\Delta y}{\nu} < 2 \tag{13}$$

in which v is the largest velocity scale in a grid cell of size Δx by Δy. Taking as representative v scale the vertical velocity in the left-side boundary layer[1] (see also Bejan,[10] p. 120, the case "Pr > 1"), we have

$$v \sim \frac{\alpha}{H}\,\mathrm{Ra}^{\frac{1}{2}} \tag{14}$$

The maximum grid size allowed by this criterion is

$$\frac{\Delta y}{H} < 2\mathrm{Pr}\,\mathrm{Ra}^{-\frac{1}{2}} \tag{15}$$

The chosen grid spacing was even smaller, this in order to place at least four grid points inside the thinnest boundary layer region (the left-side thermal boundary layer).

The time step from one converged solution to the next, $\Delta\tau$, had to satisfy the corresponding stability criterion

$$\Delta t < \frac{(\Delta y)^2}{2\nu} \tag{16}$$

which translates into

$$\Delta\tau < 2\,\frac{\mathrm{Pr}}{\mathrm{Ra}} \tag{17}$$

For example, in the solution obtained for Ra = (1.4)10⁴ and Pr = 7 the time step $\Delta\tau$ was set equal to (3.02)10⁻⁴.

The effect of grid fineness on the accuracy of the reported numerical solutions is illustrated in Figure 2, which shows how the overall Nusselt number calculated over the heated wall decreases as the time increases. The overall Nusselt number is defined as

$$\mathrm{Nu} = \frac{Q}{kH\,\Delta T/L} \tag{18}$$

where Q is the total instantaneous heat transfer rate from the heated wall per unit length normal to the plane of Figure 1. In the dimensionless notation employed in the numerical formulation of the problem, Equation 18 becomes

$$\mathrm{Nu} = \frac{1}{A}\int_0^1 -\left(\frac{\partial\theta}{\partial X}\right)_{X=0} \mathrm{d}Y \tag{19}$$

The grid size effect on Nu is shown by the detailed drawing corresponding to $\tau_L = 0.04$, where τ_L is a dimensionless time whose definition is recommended by the time scale of late stages of the transient phenomenon (see Equation 35). The late-transient dimensionless time τ_L is proportional to the time τ defined in Equation 6,

$$\tau_L = \tau\,\frac{A}{4}\,\mathrm{Ra}^{\frac{1}{2}} \tag{20}$$

There are two converging curves shown in the detail added to Figure 2. The lower curve is based on Equation 19, that is, by integrating the heat flux over the left wall. The upper curve represents the rate of increase of the bulk temperature of the enclosed fluid, as calculated at the preceding time step. This construction is based on invoking the first-law argument that the instantaneous heat transfer rate into the box is equal to the rate of internal energy accumulation inside the box. (The same argument serves as basis for the concept of "effectiveness" defined in the next section.) The discrepancy between the two estimates decreases gradually as the grid becomes finer. In the case of the 41 × 41 grid that was used for generating the solutions shown in Figures 3–6, the difference between the two Nu estimates is approximately 2%.

Numerical results

Figures 3 and 4 illustrate the main features of the transient heating by natural convection of the cavity fluid. The numbers listed on the streamlines and the isotherms indicate the values of the computed Ψ and θ values.

At relatively low Rayleigh numbers, Figure 3, the circulation consists of a single roll whose center is located near the geometric center of the cavity. This flow pattern persists throughout the τ_L interval spanned by the life of the phenomenon. The isotherm patterns show that in the beginning the temperature field develops in a manner similar to the pure conduction problem triggered by a step change in the surface temperature of a semi-infinite solid. The isotherms gradually acquire a tilt, because of the clockwise circulation. Finally, at τ_L values of order 1 the bulk temperature of the cavity fluid approaches the temperature imposed along the heated wall. The natural circulation dies down on account of the vanishing wall–fluid temperature difference, and, because of this, the heat transfer process favors again the conduction-dominated mode (note the return to nearly vertical isotherms in the last τ_L frame of Figure 3).

At higher Rayleigh numbers, Figure 4, the flow and temperature fields become considerably more interesting. The formation

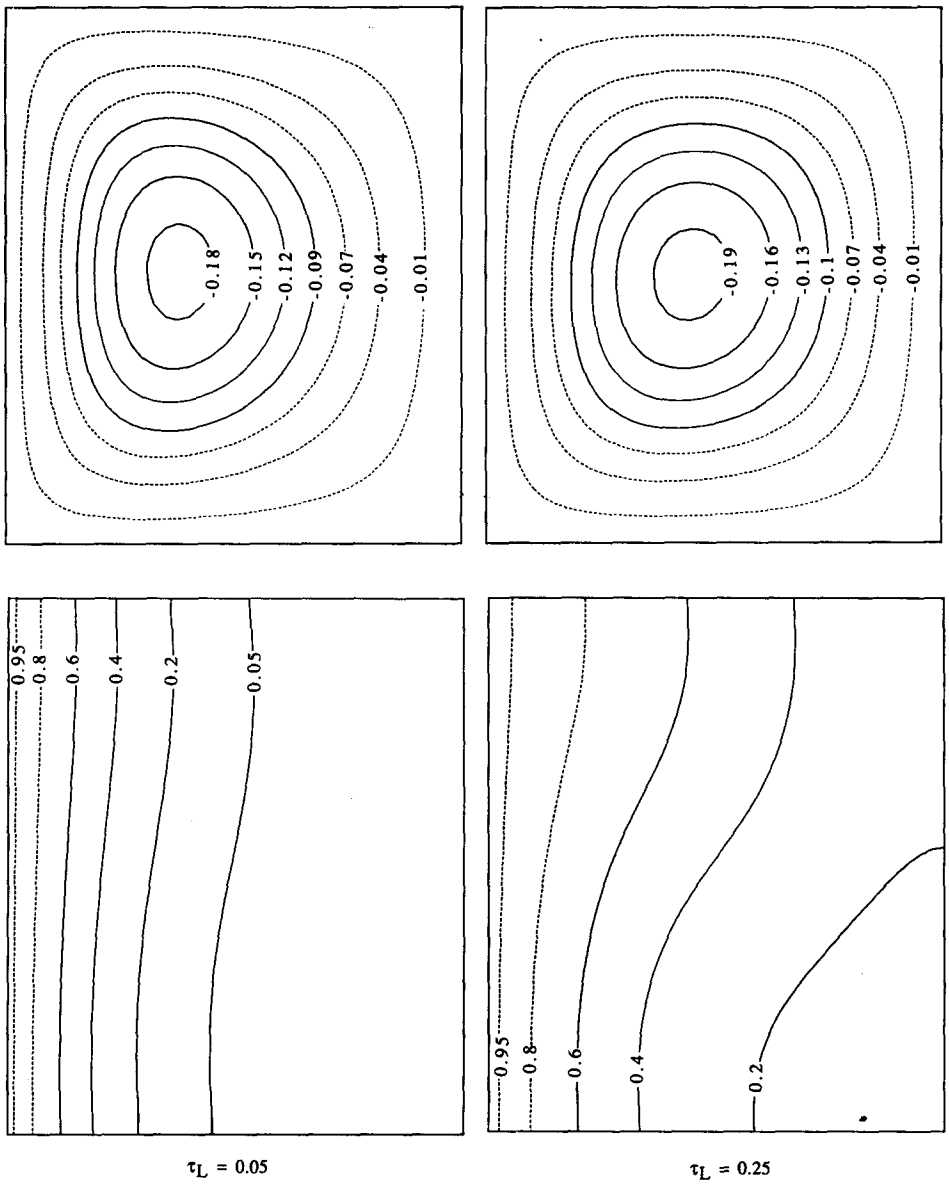

Figure 3 The evolution of the streamline and isotherm patterns when Ra = (1.4)10³, Pr = 7, and $A = 1$

and persistence of a distinct vertical boundary layer along the heated wall is evident. The discharge from this vertical jet forms initially a horizontal intrusion layer that proceeds along the top of the enclosure. This stage is shown clearly by the isotherms of the $\tau_L = 0.03$ frame, which, incidentally, look very similar to the motion-picture interferograms reported by Lee and Kauh.[4] As pointed out recently by Otis,[5] the heating of the "core" of the cavity is effected by the horizontal flow (detrainment, or negative entrainment) out of the vertical jet that is heated by the left wall. The result of this detrainment is the formation of a thermally stratified core whose temperature increases monotonically at all altitudes, even though the stratification persists. The "eye" of the circulation is noticeably closer to the heated wall throughout the τ_L interval documented in Figure 4. Once again, a τ_L value of order 1 marks the end of the transient natural convection phenomenon.

The history of the overall heat transfer rate through the left wall is summarized as Nu versus τ_L in Figure 5. Each curve is bordered at $\tau_L = 0$ by the pure conduction asymptote $\mathrm{Nu} \to \infty$ and at $\tau_L \gg 1$ by the isothermal steady-state asymptote $\mathrm{Nu} \to 0$. Desite the existence of these common asymptotes, it appears that the Nu (τ_L) curves do not have the same shape in the time interval $0 < \tau_L < 1$. Indeed, the scale analysis of the next section shows that the scaling law (i.e., the "shape") of the Nu curve changes as the time increases and as more of the cavity fluid feels the heating supplied through the left wall.

The extent to which the cavity fluid has absorbed (stored) the energy of which it is capable is documented in Figure 6 by plotting against τ_L the internal energy change fraction, called "effectiveness" for short,

$$\varepsilon = \frac{1}{\rho c H L \Delta T} \int_0^t Q \, dt \tag{21}$$

The effectiveness ε increases from $\varepsilon = 0$ (at $\tau_L = 0$) to $\varepsilon = 1$ when τ_L is sufficiently greater than 1. Figure 6 suggests that the use of τ_L on the abscissa is an effective means of correlating the effectiveness history information. We learn next that this correlation method breaks down in the early stages of the phenomenon.

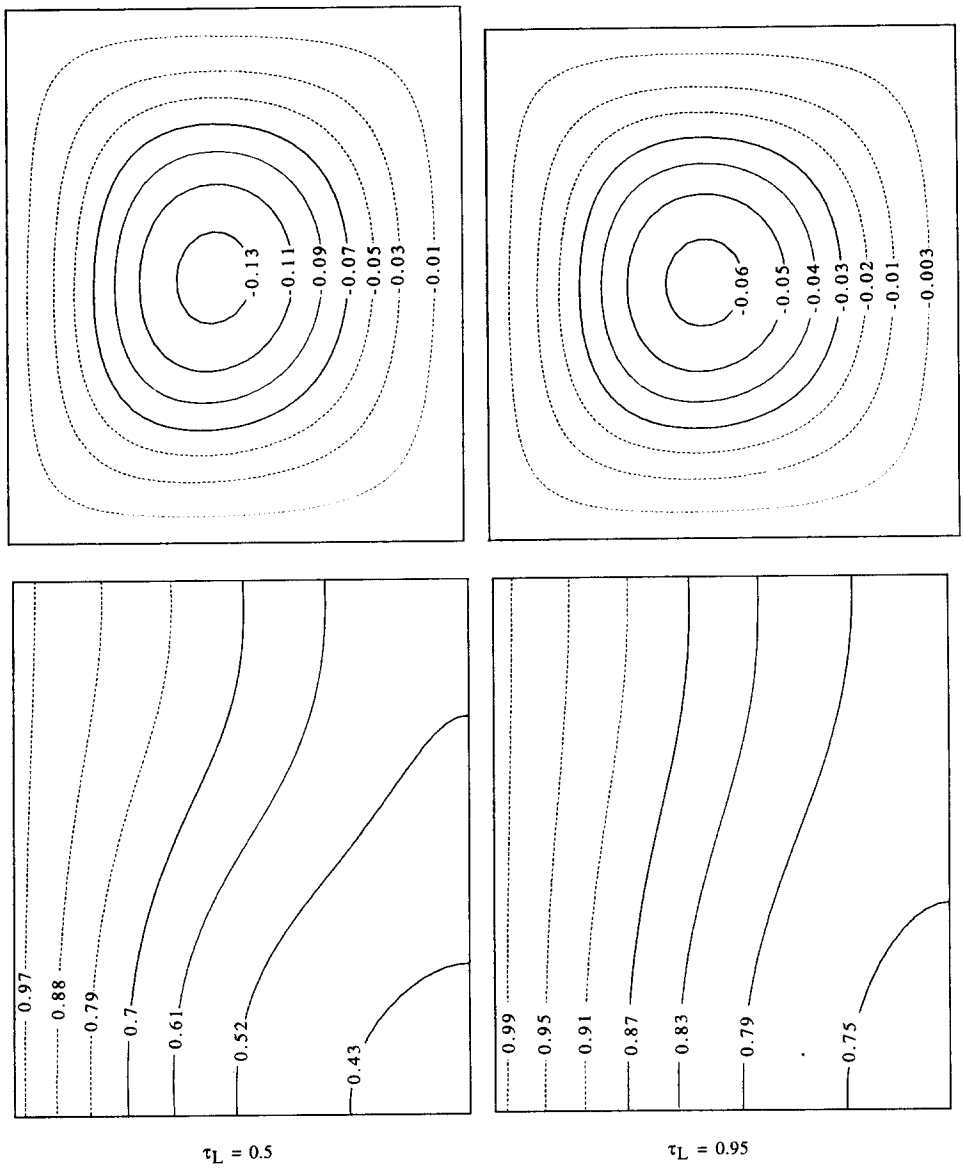

Figure 3 (continued)

Scale analysis of the early period

Immediately after $t=0$ the heated wall develops a thermal boundary layer whose thickness grows by pure conduction (that thickness is $(\alpha t)^{\frac{1}{2}}$). It has been shown by Patterson and Imberger[1] that if $\mathrm{Pr}>1$ this initial conduction layer becomes a convection boundary layer at a time of order

$$t_t \sim \frac{H^2}{\alpha}\,\mathrm{Ra}^{-\frac{1}{2}} \tag{22}$$

The $\mathrm{Pr}>1$ assumption means that in the thermal boundary layer the momentum balance is between buoyancy and friction (see also Ref. 10, p. 163).

We focus first on the early part of the transient, $0<t<t_t$, when the heat transfer through the left wall is dominated by conduction. In this regime the instantaneous overall heat transfer rate is of order

$$Q \sim kH\frac{\Delta T'}{(\alpha t)^{\frac{1}{2}}} \tag{23}$$

where $\Delta T'$ is the temperature difference between the wall and the instantaneous bulk temperature of the cavity fluid. This temperature difference decreases in time and (it can be shown quite easily) the decrease is directly related to the increase in effectiveness,

$$\varepsilon = 1-\frac{\Delta T'}{\Delta T} \tag{24}$$

Eliminating $\Delta T'$ between Equations 23–24, and then integrating 21 in which $\varepsilon=0$ at $t=0$, we obtain a relation of the form

$$\varepsilon = 1-\exp\left[-\frac{2c_1}{L}(\alpha t)^{\frac{1}{2}}\right] \tag{25}$$

In keeping with the rules of scale analysis we write c_1 in place of the unknown coefficient, which by definition is a numerical factor of order 1.

It is helpful to define at this point a new dimensionless time

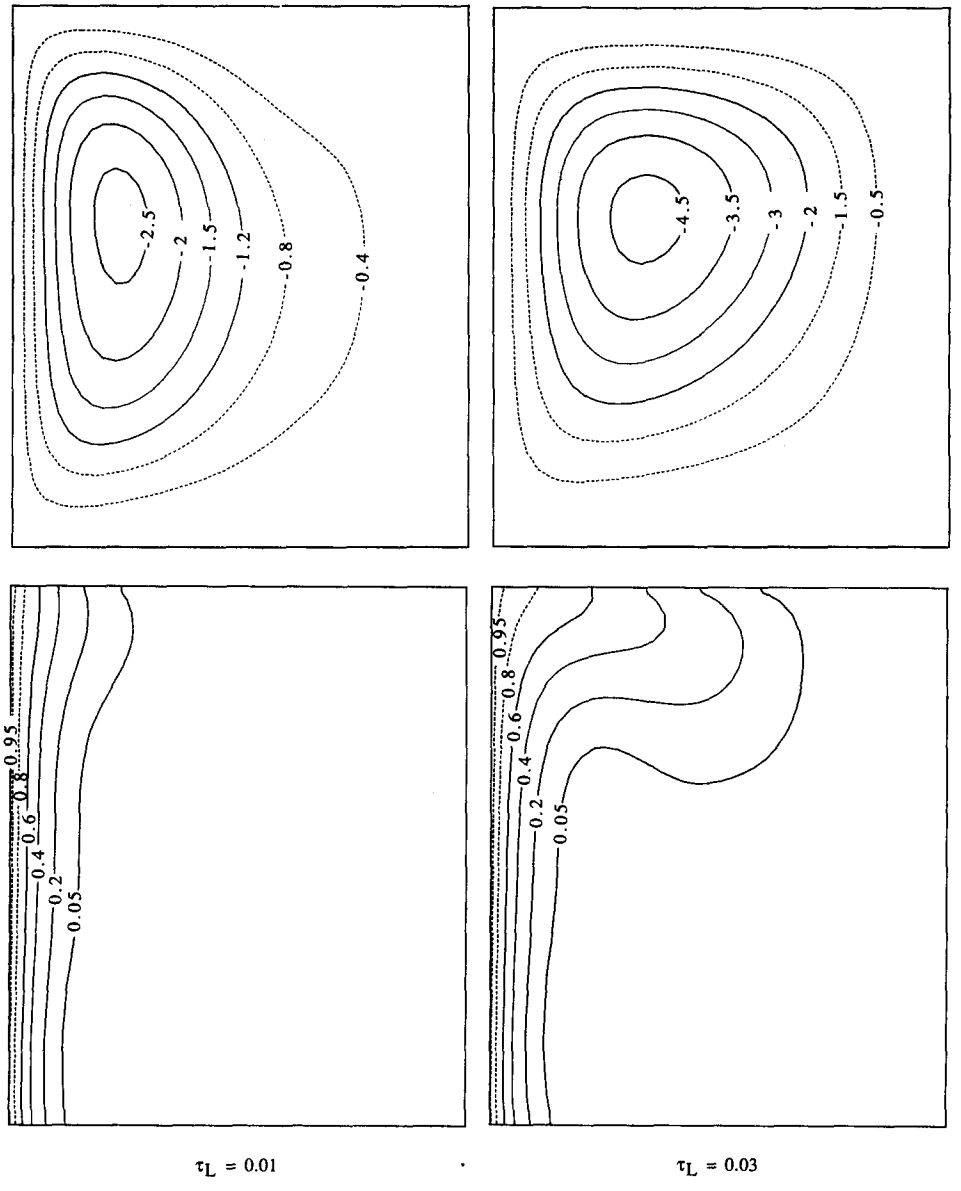

Figure 4 The evolution of the streamline and isotherm patterns when Ra = (1.4)10⁶, Pr = 7, and $A = 1$

τ_E for the "early" period,

$$\tau_E = \frac{t}{t_f} = \tau \mathrm{Ra}^{\frac{1}{4}} \tag{26}$$

which (the scaling theory says) should be of order 1 when the heat transfer mechanism is no longer dominated by conduction. Combining this with Equation 25 and rearranging yields

$$-\frac{1}{2c_1 A}\mathrm{Ra}^{\frac{1}{4}} \ln(1-\varepsilon) = \tau_E^{\frac{1}{2}} \tag{27}$$

This result suggests that the early effectiveness values calculated numerically must fall on a single curve when plotted as $\mathrm{Ra}^{\frac{1}{4}} \ln(1-\varepsilon)$ versus τ_E, and that on a log-log plot the slope of this single curve (a line, actually) should be 1/2. Indeed, Figure 7 shows that a relation of type (27) correlates successfully all the ε data in the time domin $\tau_E < O(1)$ and the Ra domain 10^3–10^6. There is a "knee" in this curve, beyond which the slope increases above 1/2. In accordance with the time criterion (22), this knee is located at $\tau_E \sim O(1)$.

Starting with Equation 23, the scale of the instantaneous overall Nusselt number for the early period can be deduced and expressed as

$$\mathrm{Nu} \sim A^{-1} \mathrm{Ra}^{\frac{1}{4}} \tau_E^{-\frac{1}{2}} \tag{28}$$

This means that the Nu data should fall on a single line of slope $-1/2$ when plotted as $\log(\mathrm{Nu} A \mathrm{Ra}^{-\frac{1}{4}})$ versus $\log(\tau_E)$. Figure 8 shows that this is indeed the case and that the correlation breaks down at times greater than $\tau_E \sim O(1)$.

Scale analysis of the late period

In this section we consider the times greater than the t_f scale (22), when the thermal boundary layer that covers the left wall is ruled by an energy balance between horizontal conduction and vertical convection.[1] It is known that the thermal boundary layer thickness in this regime scales as H times the "Rayleigh number" raised to the power $-1/4$. The distinguishing feature of the present problem, however, is that the temperature difference ($\Delta T'$) on which this Rayleigh number would be based is time-dependent. In other words, the left-wall thermal boundary

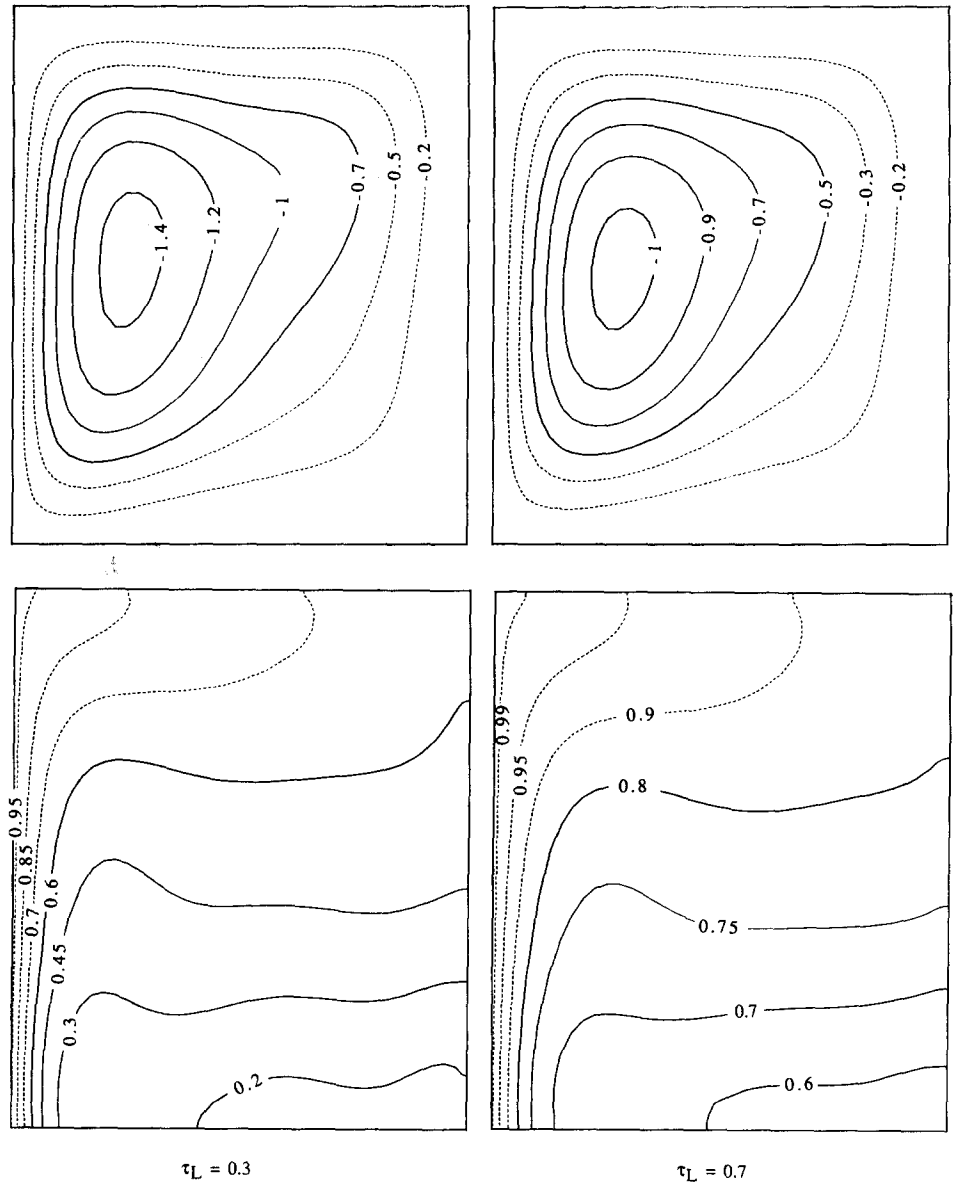

Figure 4 (continued)

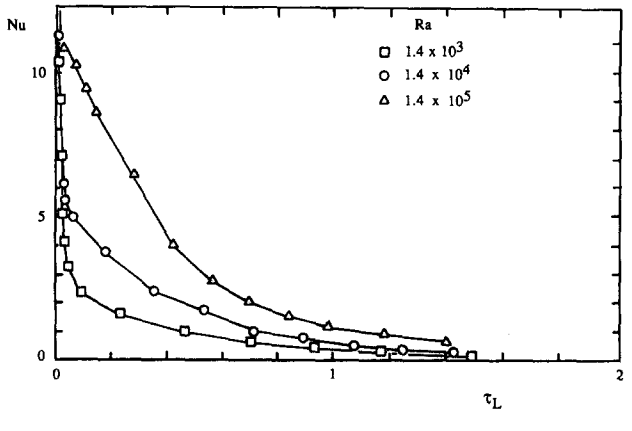

Figure 5 The effect of Ra on the history of the overall heat transfer rate

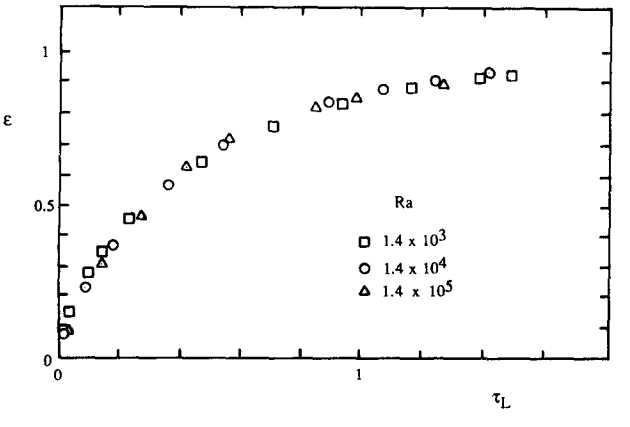

Figure 6 The effect of Ra on the history of the energy storage fraction (effectiveness)

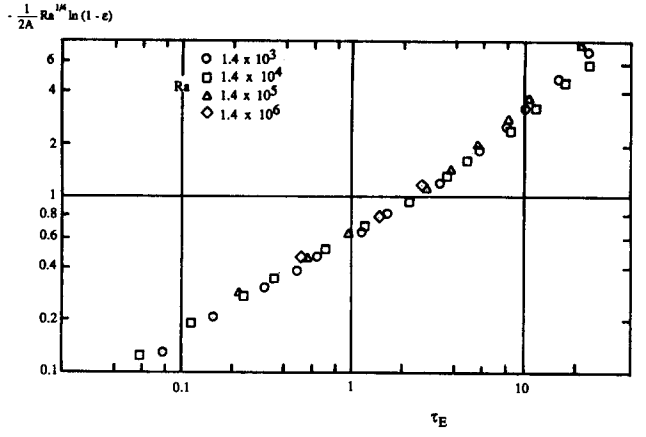

Figure 7 The early-period correlation of the numerical effectiveness data

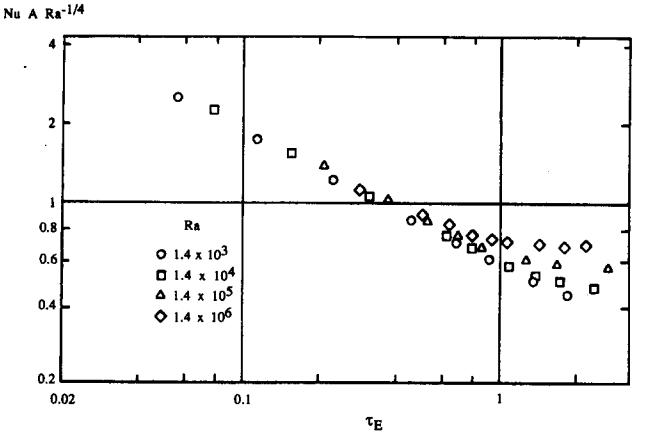

Figure 8 The early-period correlation of the numerical overall Nusselt number data

layer thickness is of order $H\mathrm{Ra}_*^{-\frac{1}{4}}$, where Ra_* is an "instantaneous" Rayleigh number whose relationship with Ra is

$$\mathrm{Ra}_*=\frac{\Delta T'}{\Delta T}\mathrm{Ra} \tag{29}$$

The analysis is essentially the same as in the preceding section, except that in place of Equation 23 for the instantaneous overall heat transfer rate we write

$$Q\sim kH\frac{\Delta T'}{H\mathrm{Ra}_*^{-\frac{1}{4}}} \tag{30}$$

Equation 24 continues to hold. By eliminating $\Delta T'$ between Equations 30 and 24, we can recast the efficiency definition (21) into the form

$$\int_0^{\varepsilon}(1-\varepsilon)^{-5/4}\,d\varepsilon\sim\frac{\alpha}{HL}\mathrm{Ra}^{\frac{1}{4}}\int_0^t dt \tag{31}$$

It is being assumed that the regime (late period) under consideration begins at $t\cong 0$ (when $\varepsilon\cong 0$), i.e., that the early period of the preceding section is much shorter than the late period. The validity of this assumption is verified at the end of this section.

Integrating both sides of Equation 31, we learn that in the late period the effectiveness should increase as

$$\varepsilon\sim 1-\left[1+\frac{\alpha t}{4HL}\mathrm{Ra}^{\frac{1}{4}}\right]^{-4} \tag{32}$$

or, more precisely, as

$$\varepsilon=1-\left[1+c_2\frac{\alpha t}{4HL}\mathrm{Ra}^{\frac{1}{4}}\right]^{-4} \tag{33}$$

where c_2 is another numerical coefficient of order 1. The first implication of this result is that the transient heating process is practicaly over ($\varepsilon\approx 1$) when the second term in brackets begins to dominate, that is, when $t>t_\infty$, where

$$t_\infty\sim 4\frac{HL}{\alpha}\mathrm{Ra}^{-\frac{1}{4}} \tag{34}$$

In terms of the late-period dimensionless time τ_L,

$$\tau_L=\frac{\alpha t}{4HL}\mathrm{Ra}^{\frac{1}{4}}=\frac{A}{4}\mathrm{Ra}^{\frac{1}{4}}\tau \tag{35}$$

the effectiveness relation (33) reads

$$(1-\varepsilon)^{-\frac{1}{4}}-1=c_2\tau_L \tag{36}$$

suggesting that the numerical ε data might be correlated as a straight line of slope 1 in the plane formed by $\log[(1-\varepsilon)^{-\frac{1}{4}}-1]$ versus $\log\tau_L$. Figure 9 confirms this idea very well, showing further that this correlation method breaks down at time τ_L less than $O(1)$.

The Nu scale in the late period follows in a few steps from Equations 30, 24, and 36:

$$\mathrm{Nu}\sim A^{-1}\mathrm{Ra}^{\frac{1}{4}}(1+c_2\tau_L)^{-5} \tag{37}$$

The correctness of this scaling law is tested in Figure 10, the construction of which proceeded from reading Equation 37 as

$$(\mathrm{Nu}A\mathrm{Ra}^{-\frac{1}{4}})^{-1/5}-1=c_2\tau_L \tag{38}$$

The figure shows clearly that the left-hand side of Equation 38 becomes proportional to τ_L at times of order $\tau_L\sim O(1)$ and greater. The value of the proportionality constant c_2 in this range is approximately 0.832.

It remains to verify that what we called "late period" lasts much longer than the early period, which was treated first. This assertion is correct if, in an order of magnitude sense,

$$t_\infty>t_f \tag{39}$$

Recognizing Equations 22 and 34, we see that the above

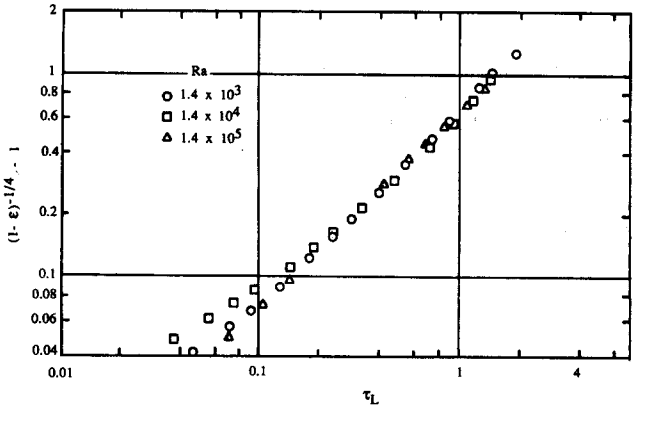

Figure 9 The late-period correlation of the numerical effectiveness data

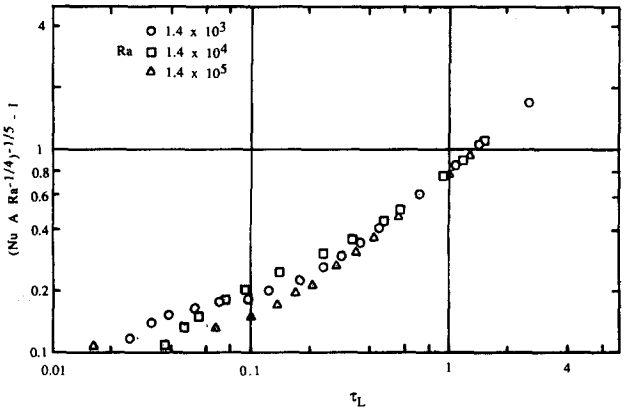

Figure 10 The late-period correlation of the numerical overall data

criterion translates into

$$4\mathrm{Ra}^{\frac{1}{4}} > A \tag{40}$$

which is certainly confirmed by the (Ra, A) domain covered by the numerical experiments described in the first part of the paper (Figures 3–6).

Conclusions

The transient natural convection heating of an enclosed fluid was analyzed by recognizing the two heat transfer mechanisms that compete during the process. In the "early" period, which is represented by the time criterion $t < t_f$, the heat transfer through the side wall is dominated by conduction. During the "late" period ($t > t_f$) the heating from the side is predominantly convective. The instantaneous Rayleigh number Ra_* (based on $\Delta T'$) decreases steadily as t increases. Consequently, the fluid approaches a uniform temperature, and the process is again dominated by conduction. This particular time scale is associated with the time when the side-wall thermal boundary layer thickness $H\mathrm{Ra}_*^{-\frac{1}{4}}$ has grown to be comparable with H, i.e., when

$$\mathrm{Ra}_* \sim O(1) \tag{41}$$

or, via Equation 29,

$$\frac{\Delta T'}{\Delta T} \sim \mathrm{Ra}^{-1} \tag{42}$$

Substituting into this condition Equations 24 and 33 leads finally to

$$\tau \sim \frac{4}{A} \tag{43}$$

This time scale can be compared with the time when the cavity stores practically all the energy of which it is capable ($\varepsilon \sim 1$). Then, by setting $\tau_L \sim 1$ in Equation 35, $\tau \sim (4/A)\mathrm{Ra}^{-\frac{1}{4}}$. Since $\mathrm{Ra} \gg 1$, we conclude that the time scale given by Equation 43 is longer than the time when $\varepsilon \sim 1$. The time scale that separates the early period (fifth section in this paper) from the convective period (sixth section) is $t \sim t_f$, which corresponds to $\tau \sim \mathrm{Ra}^{-\frac{1}{4}}$.

As an engineering summary to this study, the scaling-correct correlations for ε and Nu are

$$\varepsilon = \begin{cases} 1-\exp(-1.144A\tau^{\frac{1}{4}}), & \tau < \mathrm{Ra}^{-\frac{1}{4}} \\ 1-(1+0.208\mathrm{Ra}^{\frac{1}{4}}A\tau)^{-4}, & \tau > \mathrm{Ra}^{-\frac{1}{4}} \end{cases} \tag{44}$$

$$\mathrm{Nu} = \begin{cases} 0.591A^{-1}\tau^{-\frac{1}{4}}, & \tau < \mathrm{Ra}^{-\frac{1}{4}} \\ 0.847A^{-1}\mathrm{Ra}^{\frac{1}{4}}(1+0.208\mathrm{Ra}^{\frac{1}{4}}A\tau)^{-5}, & \tau > \mathrm{Ra}^{-\frac{1}{4}} \end{cases} \tag{45}$$

These expressions contain the numerical coefficients of order 1 mentioned during the scale analysis, which have been determined empirically based on the numerical results described in the third and fourth sections. One noteworthy feature of these correlations is that they do not contain Pr as an independent parameter. This feature is a reflection of the "$\mathrm{Pr} > 1$" assumption made early on in the scale analysis of the convection-dominated period. The chief contribution of the scale analysis of boundary layer natural convection in $\mathrm{Pr} > 1$ fluids is the conclusion that the relevant dimensionless group is the Rayleigh number, i.e., that the Prandtl number and the Grashof number always participate as a product (Ref. 10, pp. 116–118).

In using the correlations (44, 45), one should keep in mind that they are based on the assumption of constant properties. In reality, the group $\beta/\alpha\nu$ for water increases by roughly 25% as the temperature changes from 25 to 30°C (Ref. 10, p. 463). Under the same conditions, the group $\beta/\alpha\nu$ for dry air decreases by approximately 8% (Ref. 10, p. 465). Therefore, the conclusions of this study can be regarded as only approximate in applications in which the initial temperature difference between wall and fluid is greater than 5°C.

References

1 Patterson, J. C. and Imberger, J. Unsteady natural convection in a rectangular cavity. *J. Fluid Mechanics*, 1980, **100**, 65–86

2 Yewell, R., Poulikakos, D., and Bejan, A. Transient natural convection experiments in shallow enclosures. *J. Heat Transfer*, 1983, **106**, 533–538

3 Ivey, G. N. Experiments on transient natural convection in a cavity. *J. Fluid Mechanics*, 1984, **144**, 389–401

4 Lee, T. S. and Kauh, S. Unsteady natural convection in a rectangular enclosure. Heat Transfer: Korea–USA Seminar Proceedings, Department of Mechanical Engineering, Seoul National University, October 16–22, 1986, 51–63

5 Otis, D. R. Convection as the dominant mechanism of core stratification during transient natural convection in enclosures at high Rayleigh numbers. *Int. Comm. Heat Mass Transfer*, 1987, **14**, 597–604

6 Patterson, J. C. On the existence of an oscillatory approach to steady natural convection in cavities. *J. Heat Transfer*, 1984, **106**, 104–108

7 Nicolete, V. F., Yang, K. T., and Lloyd, J. R. Transient cooling by natural convection in a two-dimensional enclosure. *Int. J. Heat Mass Transfer*, 1985, **28**, 1721–1732

8 Peaceman, D. W. and Rachford, H. H. The numerical solution of parabolic and elliptic differential equations. *J. Soc. Ind. Appl. Math.*, 1955, **3**, 28–41

9 Roache, P. J. *Computational Fluid Dynamics*, Hermosa, Albuquerque, 1976

10 Bejan, A. *Convection Heat Transfer*, Wiley, New York, 1984